Earthquakes and Structures, *Vol. 8, No. 3 (2015) 665-679*
DOI: http://dx.doi.org/10.12989/eas.2015.8.3.665

Effect of loading velocity on the seismic behavior of RC joints

Licheng Wang*, Guoxi Fan[a] and Yupu Song[b]

State Key Laboratory of Coastal and Offshore Engineering, Dalian University of Technology, Dalian, China

(Received January 14, 2014, Revised May 16, 2014, Accepted July 13, 2014)

Abstract. The strain rate of reinforced concrete (RC) structures stimulated by earthquake action has been generally recognized as in the range from 10^{-4}/s to 10^{-1}/s. Because both concrete and steel reinforcement are rate-sensitive materials, the RC beam-column joints are bound to behave differently under different strain rates. This paper describes an investigation of seismic behavior of RC beam-column joints which are subjected to large cyclic displacements on the beam ends with three loading velocities, i.e., 0.4 mm/s, 4 mm/s and 40 mm/s respectively. The levels of strain rate on the joint core region are correspondingly estimated to be 10^{-5}/s, 10^{-4}/s, and 10^{-2}/s. It is aimed to better understand the effect of strain rates on seismic behavior of beam-column joints, such as the carrying capacity and failure modes as well as the energy dissipation. From the experiments, it is observed that with the increase of loading velocity or strain rate, damage in the joint core region decreases but damage in the plastic hinge regions of adjacent beams increases. The energy absorbed in the hysteresis loops under higher loading velocity is larger than that under quasi-static loading. It is also found that the yielding load of the joint is almost independent of the loading velocity, and there is a marginal increase of the ultimate carrying capacity when the loading velocity is increased for the ranges studied in this work. However, under higher loading velocity the residual carrying capacity after peak load drops more rapidly. Additionally, the axial compression ratio has little effect on the shear carrying capacity of the beam-column joints, but with the increase of loading velocity, the crack width of concrete in the joint zone becomes narrower. The shear carrying capacity of the joint at higher loading velocity is higher than that calculated with the quasi-static method proposed by the design code. When the dynamic strengths of materials, i.e., concrete and reinforcement, are directly substituted into the design model of current code, it tends to be insufficiently safe.

Keywords: reinforced concrete (RC) beam-column joints; seismic behavior; loading velocity; shear carrying capacity; failure mode

1. Introduction

The seismic response of reinforced concrete (RC) beam-column joints, which are the critical regions in a RC frame structure, is of prime importance especially when subjected to heavy earthquake action. As a result, the seismic behavior of RC beam-column joints has been wide studied in the past few decades (Hakuto *et al*. 2000, Li and Tran 2009, Li *et al*. 2009, Meas *et al*.

*Corresponding author, Professor, E-mail: wanglicheng2000@163.com
[a]Ph.D. Student
[b]Professor

http://www.techno-press.org/?journal=eas&subpage=7 ISSN: 2092-7614 (Print), 2092-7622 (Online)

2014). It has also been found that the dynamic loading effect caused by earthquake action plays a crucial role on the response and performance of beam-column joints (Shah *et al*. 1987). However, the majority of current design codes used for seismic analysis of RC beam-column joints are mainly based on the quasi-static test results. The orders of magnitude of strain rate in quasi-static tests are usually lower than those excited by earthquake, which are generally recognized in the range between 10^{-4}/s and 10^{-1}/s,. Extensive work has been conducted over the past decades to study the dynamic properties of concrete. The obtained results have reported that concrete is a rate-sensitive material, indicating that both its strength and stiffness depend on the strain rate/loading rate (Hasan *et al*. 2010, Cusatis 2011, Boyce and Dilmore 2009). Bischoff and Perry (1991) summarized the effect of loading velocity on the concrete compressive strength, and pointed out that there was much uncertainty about the effect of various testing techniques mainly due to the different boundary conditions. Despite this, a definite increase in compressive strength of concrete, as the strain rate is increased, has generally been accepted. Malvar and Ross (1998) investigated the influence of loading velocity on the dynamic tensile strength of concrete. Thereafter, to well account for the strain rate effect of concrete in the design process, many design codes have already given their models for predicting the concrete dynamic strength. For example, the CEB-FIP Model Code (1991) proposed the formulations to evaluate the dynamic properties of concrete by updating static properties, in which the quasi-static strain rates were respectively set as 30×10^{-6}/s for compression and 1×10^{-6}/s for tension.

Metallic materials, such as steel, are also found to be sensitive to the rate of loading. For example, Manjoine (1944) conducted strain-rate tests on mild steels at room temperature for strain rates from 9.5×10^{-7}/s to 3×10^{2}/s. These test results indicated that the yield strength of mild steel increased with an increase of strain rate, especially for strain rates greater than 10^{-1}/s. Sun *et al*. (2003) developed physical equations to represent the strain rate dependencies of the Lüders strain and the Lüders-band velocity for annealed mild steel. In their equations, both the Lüders strain and the Lüders-band velocity increased with strain rate in the form of exponent functions. Lee *et al*. (2009) investigated the impact behavior of sintered 316 L stainless steel at strain rates ranging from 10^{-3}/s to 7.5×10^{3}/s and found that the flow stress-strain response of the sintered 316 L stainless steel depended strongly on the applied strain rate. In addition, experimental measurements of the plastic deformation behavior over a wide variety of pure metals and alloys have been carried out in order to study the effect of strain rate. The findings of these works have shown that for a given plastic strain, the flow stress is linearly related to the natural logarithm of the strain rate ranging from approximately 10^{-3}/s to 10^{3}/s (Mukai *et al*. 1995, Lee *et al*. 2000, Lee and Lin 1998).

In view of the efforts in the literature, previous studies concerned more about the stress or strain rate effect on material property of concrete and steels. Research works related to the rate effect on seismic performance of RC members are mainly focused on numerical methods (Sharma *et al*. 2011, Ghobarah and Biddah 1999). Shah *et al*. (1987) investigated the carrying capacity and energy dissipation of exterior beam-column joints at different loading rates through three small-scale model specimens. More recently, Li and Li (2012) studied the effect of loading rate on the bending carrying capacity and deformation properties of freely supported beams with two different shear span ratios. Isaac *et al*. (2013) proposed a method for predicting the shear behavior of a RC beams when subjected to impact loads by taking into account the impact velocity. On the basis of comparisons between fast and slow rates of loading tests, it was found that at the faster rate, the maximum load carrying capacity of the member is higher, but it usually induced a larger amount of energy dissipation. Also, it was concluded that faster loading speed will cause greater damage when compared with slow rate. For more general sense, however, there is a lack of experimental and theoretical investigation on the seismic behavior of RC interior beam-column joints when the strain rate effect is taken into account.

In the present paper, seven full scale cruciform joint specimens were prepared. The large cyclic displacements were applied on beam ends of the beam-column joint with three different loading velocities, i.e., 0.4 mm/s, 4 mm/s and 40 mm/s respectively. In terms of the test observations and recorded results, the effect of loading velocity and axial compression ratio on the seismic behavior, such as the failure mode, carrying capacity and energy dissipation, were discussed.

2. Experimental program

2.1 Specimen design

When a RC frame structure is encountered to horizontal seismic loading, the distribution of bending moment around an interior beam-column joint is depicted in Fig. 1. If the multistory frame structure with the same story height is subjected to horizontal loading, the contraflexure points are usually located in the 1/2 beam span and l/2 column height. The intersection part between beam and column is referred to as the core region of a beam-column joint. As a result, the joint core region, portion of beams and columns selected from the contraflexure points to member ends adjacent to the core region, make up the beam-column joint combination specimen. Therefore, the length of beam and column on both sides of the joint core region may be selected equaling to 1/2 beam span and l/2 column height, respectively (Shah *et al*. 1987).

The uniform cross sections for all joint specimens, i.e., the rectangular cross section for beams and square cross section for columns, are designed with beams continuously passing through the column panel zone. Fig. 2 shows the loading system and reinforcement details of specimens. The flextural carrying capacity of column and beam are designed in accordance with M_c>1.4M_b, where M_c and M_b represent the flextural carrying capacity of the column and beam respectively. The “strong column-weak beam” philosophy is recommended to ensure the formation of beam plastic hinging rather than column plastic hinging at large displacement levels (Lu *et al*. 2012). Also, the ultimate carrying capacity of the beam-column joint should be greater than the flexural yielding strength of the adjacent beam and column, and should not degrade before the beam reaching its required ductility. So it allows the beam to form plastic hinge adjacent to beam-column joint.

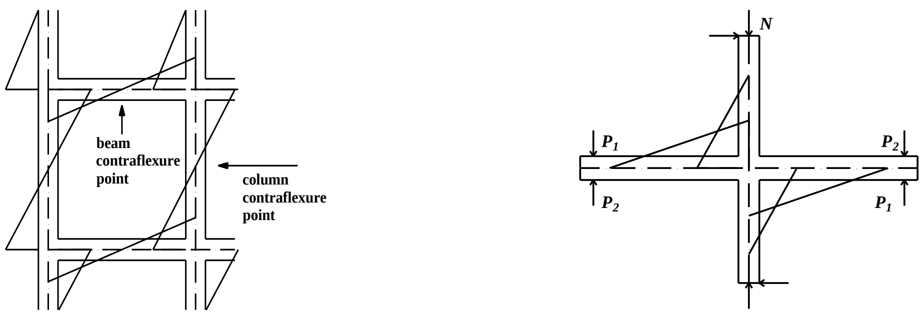

(a) Distribution of bending moment of a frame (b) Loading details of a joint

Fig. 1 Schematic diagram of the joint design

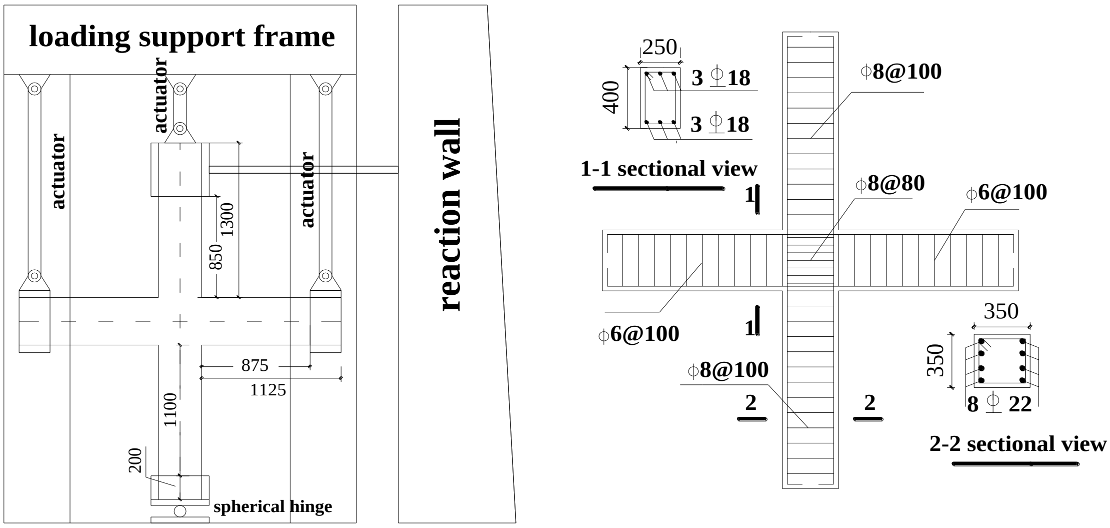

(a) Loading system for a joint specimen (b) Designed details

Fig. 2 Loading system and designed details of the specimens

Table 1 Material properties for the specimens

Yield strength of beam longitudinal reinforcement (MPa)	Diameter of beam longitudinal reinforcement (mm)	Yield strength of column longitudinal reinforcement (MPa)	Diameter of column longitudinal reinforcement (mm)	Yield strength of stirrup reinforcement (MPa)	Diameter of stirrup reinforcement (mm)
367.7	18	342.3	22	305/481	6/8

All the specimens were cast at a time from the same batch of concrete with the same wet-cured conditions to ensure same concrete properties. The prismatic compressive strength of concrete at 28 days was 25.24 MPa. All the specimens have the same longitudinal reinforcements and stirrups with a concrete cover of 30 mm. The material properties are listed in Table 1.

2.2 Test setup and loading apparatus

Fig. 3 shows a cruciform specimen fixed on the apparatus before testing. The column top is fixed through steel brace to the loading support frame in order to guarantee the stability of the joint specimen both in plane and out of plane. The column top and bottom are supported by spherical hinges. In addition, to realize the reversal of tension and compression loading, the steel plates and connecting bolts are used to connect the actuators and the beam ends. A vertical cyclic load is applied at the end of the beam under displacement control by a vertical electro-hydraulic servo-controlled actuator with a displacement capacity of ±300 mm, while a vertical constant load is applied at the top of the column under load control by a vertical electro-hydraulic servo-controlled actuator with a load capacity of ±2000 kN.

The loading apparatus is equipped with electro-hydraulic servo control system that allows switching from the load-control mode to the strain-control mode during the test. It can

Fig. 3 A photograph showing specimen fixed in position before the test

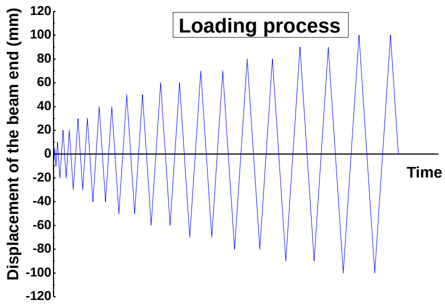

Fig. 4 Loading history of the beam-column joint

simultaneously control the actuators to apply quasi-static cyclic load or dynamic cyclic load in three directions. Before test, yield displacement of frame beam under monotonic static loading is obtained from analysis by using the finite element software. The results show that the yielding displacement at the beam end is about 10 mm. The loading history for the beam-column joints can thus be determined. Initially, the actuator on top of the column applies the corresponding axial load, according to the axial compression ratio requirement, which takes 20 s to apply the axial load up to the maximum value. This axial load will keep constant during the test. After preloading 60 s to eliminate distortion errors, the vertical electro-hydraulic servo-controlled actuators at each beam end apply the cyclic load with displacement control in the form of triangular waves, as illustrated in Fig. 4. Single cyclic loading is applied until the yielding of the beam longitudinal reinforcements. During each loading cycle run, the displacements at the top of the column are recorded on a personal computer until reaching the target displacement level. After yielding starts, loading cycles will repeat twice per displacement upon to the carrying capacity of specimen decreasing to 85% of the maximum value or to the final failure of the specimen.

During the loading cycles, the corresponding storey drift, crack widths and reinforcement strains are respectively measured by LVDTs (Linear Variable Differential Transformer) and strain gages. All cracks are marked on the white painted surface, which will be used to describe the failure mode of the specimen.

2.3 Testing program

The seven specimens are divided into two groups in order to separately study the effect of loading velocity and axial compression ratio on the seismic behavior of RC frame joints. For the first group, three specimens, i.e., QM, HM and MM, with the axial compression ratio of 0.20 were included, and the loading velocities at the end of the beams were 0.4 mm/s (regarded as quasi-static loading), 40 mm/s (high velocity of loading), 4 mm/s (medium velocity of loading), respectively. For the second group, four specimens of HM under high loading velocity were prepared to investigate the influence of axial compression ratio. The axial compression ratios were taken as 0.05, 0.10, 0.15 and 0.25 respectively.

3. Test results and discussion

3.1 Estimation of strain rate orders

As well known, the seismic behavior of structural material depends on the earthquake intensity and the structural dynamic characteristics. Typically, the strain rates experienced by the structural members are varied at different locations of a structure and different time during an earthquake excitation. However, the strain rate excited by earthquake will generally remain the order of magnitude ranging from 10^{-4} to 10^{-1}/s (Bischoff and Perry 1991). In this paper, the plastic hinge region of beam end is selected as the critical section. When the rebar of the critical section yields in the test, the time to reach the yielding state can be determined by the actual displacement and loading rate. If a linear increase is assumed for the strain to reach this yielding state, the strain rate will be estimated by the above mentioned time for the corresponding loading rate. Computed through the test results which are collected by strain gages, the orders of magnitude of the strain rate are 10^{-5}/s, 10^{-4}/s, 10^{-2}/s, corresponding to the loading rates at beam ends equaling to 0.4 mm/s, 4 mm/s and 40 mm/s, respectively.

Currently, the real strain rate orders of RC structures or members are generally estimated through an inverse method with the measured test results. This is realized in such a way: the load is applied on the specimen with a given velocity, and during the loading history, the strain history of concrete and reinforcement at some critical zones can be measured and recorded, and then the elastic stage of which will be used to evaluate the strain rate. Before loading, obviously, it is unable to precisely determine the strain rate. Since any observable differences in material properties become significant only when the strain rate is increased by one order of magnitude or greater, Asprone *et al*. (2012) proposed a method to roughly estimate the strain rate assuming a linear variation of the strain rate in loading time. In their method, the measured strains of concrete or steel reinforcement are assumed to linearly reach the maximum values when the applied maximum displacement on a structure is just achieved. Accordingly, if the spectral velocity (V) and the maximum displacement (PSD) of a RC structure or member have been known during the seismic excitation, the time to reach the maximum displacement, $T_{\max}$, can be calculated as

$$T_{\max} = \frac{PSD}{V} \tag{1}$$

As a result, when a RC structure or its member reaches the yielding displacement state in a given displacement cycle, the strain rate of the RC structure or its member can be approximated as

$$\dot{\varepsilon} = \frac{\varepsilon_y}{T_{\max}} \tag{2}$$

where ε_y represents the yielding strain of reinforcement or concrete. In terms of the above method, the strain rate orders of the RC beam-column joints in the current study are approximately estimated as 8×10^{-5}/s, 8×10^{-4}/s and 1×10^{-2}/s corresponding to the loading velocity of 0.4 mm/s, 4 mm/s and 40 mm/s respectively. Therefore, the orders of magnitude of the strain rate calculated by the two methods are very close to each other, indicating that the method proposed by Asprone *et al*. (2012) can be used to choose loading velocity prior to testing on the basis of the assumed strain rate level.

3.2 Mode of failure

To investigate the loading velocity on failure mode of the joint specimen, the cracking patterns of three cruciform specimens with identical axial compression ratio are illustrated in Figs. 5 to 7 Specimen QM, subjected to a quasi-static loading velocity (0.4 mm/s) exhibits the typical flexural shear failure. In other words, the shear failure occurs in the joint core area after plastic hinges develop at both ends of adjacent beams, with loss of carrying capacity due to the excessive deformation. During the process of loading, when the applied displacement on beam ends is 10 mm, the anti-symmetric flexural cracks appear in beams on both sides of the beam-column joint. After the cyclic displacement reaching 20 mm, the principal orthogonal diagonal cracks develop in the core area. As the applied displacement continues to increase, the specimen performs in a ductile manner with plastic hinges formed at the beam ends near the joint face, and the concrete cover below the beam longitudinal tensile reinforcement region begins to spall off followed by crushing of concrete at the compression regions of beams. In addition, a large number of inclined cracks, which are parallel to the principal diagonal cracks, develop in the core area due to the action of reciprocating shear force. After this stage, concrete cover at the central position of the joint core area gradually spalls off because of yielding of stirrups, and then, the core concrete is crushed, leading to the complete failure of the specimen. The finial failure mode of specimen QM is shown in Fig. 5.

For specimen HM, the loading velocity at beam ends is 40 mm/s. At beginning, some vertical cracks induced by the bending moment appear in the frame beams. Followed that, the diagonal cracks in the core area caused by shear force and in the frame beams caused by principal tensile

Fig. 5 Failure pattern of QM

Fig. 6 Failure pattern of HM

Fig. 7 Failure pattern of MM

stress generate almost simultaneously. Compared with specimen QM, HM has the similar failure mode. The shear failure occurs in joint core area after plastic hinges develop at both ends of adjacent beams, followed by crushing of concrete. Although there is no essential change in the failure mode, specimen HM is more inclined to brittle failure. This can be attributed to the fact that, with an increase in strain rate, shear stress tends to increase rapidly to the failure stress while flexural displacement has not yet to develop due to the shortened loading time. From Fig. 6, it can also be known that the number of cracks in specimen gradually decreases as strain rate increases. It tends to produce a few main cracks since the development of internal micro cracks is limited. It is observed that, as strain rate increases, damage in the joint core area decreases but damage in the plastic hinge regions of adjacent beams increases. Moreover, the obvious bond slip of the beam longitudinal reinforcement at the interface between beam and column is observed.

Comprehensively compared with QM (under quasi-static loading) and HM (under high velocity of loading), the failure pattern of specimen MM falls in between, as shown in Fig. 7. Cracks in the core area have better development, and the bond slip of the beam longitudinal reinforcement at beam-column interface is not as notable as that under high velocity of loading.

Some support for the above findings can be referred to the former literatures. For example, Bischoff and Perry (1991) found a decrease in internal micro cracks with an increasing strain rate. Takeda (1984) studied the rate effect on the bond stress distribution on deformed bar during a pull-out test. The results indicated that the bond stresses were more localized at higher rate. Particularly, Shah *et al*. (1987) observed that flexural cracks were widely distributed for the exterior beam-column joints at slow loading rate. In contrast, for the fast rate, the damage was essentially induced by a single wide crack at the face of the column. However, because of the more efficient load-transfer occurring at the slow rate, additional cracking progressively developed at sections further away from the column face.

3.3 Load-deflection hysteresis curves and the skeleton curves

During the test, the load-deflection hysteresis curves of each specimen were collected by means of the electro-hydraulic servo control system and the LVDTs, as shown in Fig. 8. It can be seen that the ultimate carrying capacity of specimen HM under high loading velocity is higher than that of the specimen QM under quasi-static loading, but the increased magnitude of carrying capacity is not much significant. All the load-deflection hysteresis curves of three specimens exhibit the pinching effect, and particularly for specimen HM, the pinching effect looks most evident. This can be interpreted that under large deflection, the beam longitudinal reinforcement bars in the plastic hinge zone have already yielded, and subsequently progressed to the joint core region. This process will result in the bond slip of longitudinal reinforcement bars within beam concrete.

It can also be seen from Fig. 8 that the degradation of stiffness and carrying capacity of specimen HM decline sharply after reaching its ultimate point. That is to say, the damage induced by cyclic loading is greater with the increase of strain rate, which is in accordance with the conclusion obtained by Shah *et al*. (1987).

In terms of the load-deflection hysteresis curves, the load-deflection skeleton curve can be obtained for each specimen (shown in Fig. 9). The skeleton curves can be further used to predict the variation of the carrying capacity with loading velocity. It can be seen that all specimens undergo elastic, elastic-plastic, stable as well as failure stages. When Δ=5 mm and Δ=10 mm, the increased strain rates have a beneficial influence on the carrying capacity of specimens, indicating that with an increase of strain rate, the initial stiffness of specimens is improved.

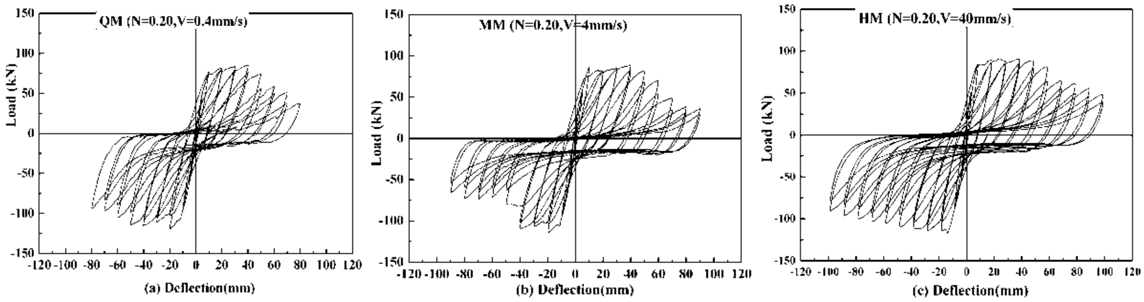

Fig. 8 Loading-deflection hysteresis curves of the specimens

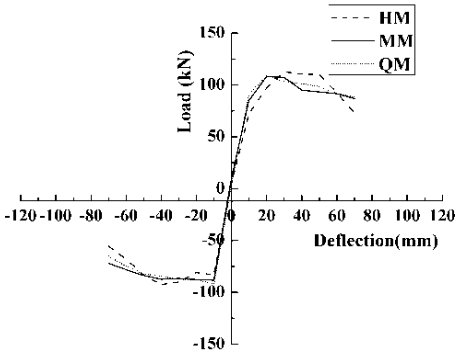

Fig. 9 Comparison of load-deflection skeleton curves among the specimens

Moreover, it is observed that the slope of post-peak branch (i.e., descending branch) of the skeleton curves increase for high loading velocities. It indicates that, after reaching the ultimate carrying capacity, the degradation of stiffness and carrying capacity are more serious as the loading velocity increases, which is unfavorable to the overall performance of the beam-column joints and the frame structures.

3.4 Energy dissipation

The energy dissipation capacity is also an important parameter to evaluate the seismic behavior of the structure. To study the energy dissipation capacity of specimens during loading process, the first hysteresis loop at each displacement level is selected, and its area is calculated by numerical integration to get the energy dissipation curves at different loading rates. The concept of equivalent viscous damping h_{eq} is proposed by Jacobson in 1930. Since then, the equivalent viscous damping h_{eq} becomes the key indicator to evaluate the energy dissipation capacity of specimens in seismic engineering. The equivalent viscous damping h_{eq} can be calculated as follows

$$h_{eq} = \frac{S_{\mathrm{ABCDEF}}}{2\pi . S_{\Delta\mathrm{OBG}+\Delta\mathrm{OEH}}} \tag{3}$$

in which S_{ABCDEF} is the area of ellipse ABCDEF and $S_{\Delta\mathrm{OBG+OEH}}$ is the area of triangle OBG and OEH. The meanings of parameters in Eq. (3) are depicted in Fig. 10. The energy dissipation and

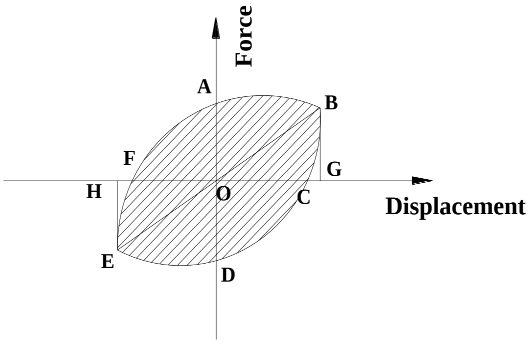

Fig. 10 Schematic illustration of the equivalent viscous damping h_{eq}

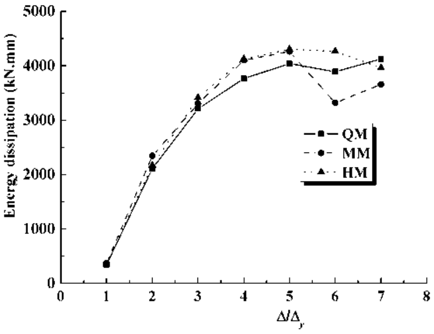

Fig. 11 Comparison of the energy dissipation under different loading velocity

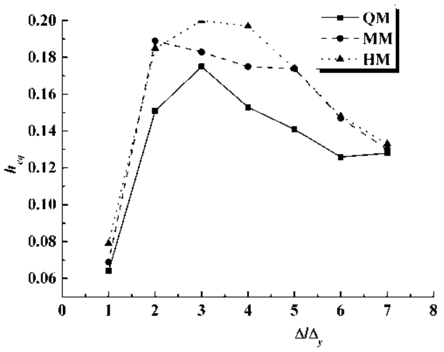

Fig. 12 Comparison of h_{eq} under different loading velocity

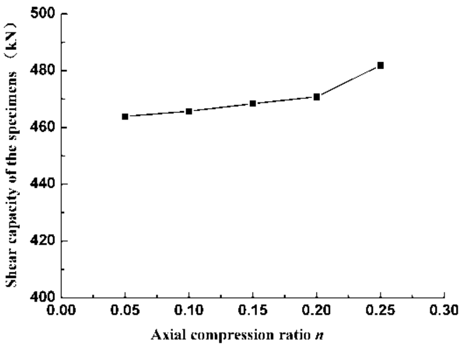

Fig. 13 Shear capacity of the specimens at different compression ratio

equivalent viscous damping of specimens under different loading rates are computed, which are given respectively in Figs. 11 and 12. It can be seen that, according to the energy dissipation and the equivalent viscous damping the specimens HM and MM dissipate more energy until their displacement ductility factor ($\mu_{\Delta}=\Delta/\Delta_y$) reaching 6.0, and especially from Fig. 12 that the values of h_{eq} for higher loading rates are obviously higher than those of the quasi-static loading case. This result indicates that the specimen is more seriously damaged as the loading rate increases. Moreover, the energy dissipation capacity of specimens HM and MM decrease rapidly after their displacement ductility factor reaching 6.0. This shows that although the carrying capacity is increased to some extend with increasing the loading velocity, the damage degree is intensified.

3.5 Influence of axial compression ratios on shear carrying capacity

Fu (2002) pointed out that, when the shear compression ratio lies in a certain range, the increase of axial compression ratio can slow down the yield penetration of beam reinforcement bars. As a result, the axial compressive stress can adequately improve the bonding conditions of beam longitudinal reinforcement bars throughout the core area of the beam-column joint, which is beneficial to the seismic performance of the overall frame. But when the axial compression ratio is further increased, due to the large compressive stress endured by diagonal strut, concrete in the

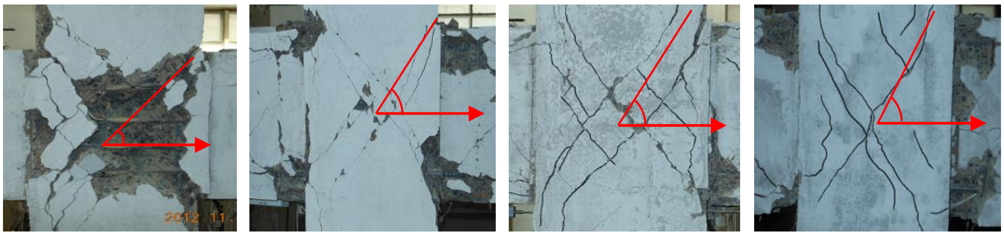

n=0.05 *n*=0.10 *n*=0.15 *n*=0.25

Fig. 14 Failure patterns of the specimens at different compression ratios

joint core area will be crushed, which reflects an adverse effect. The current work comparatively investigates the influence of axial compression ratio on the failure mode and shear carrying capacity of beam-column joints under high velocity of loading. The shear carrying capacity of beam-column joints for five different axial compression ratios (n=0.05, 0.10, 0.15, 0.20, 0.25) are shown in Fig. 13. One can see that the axial compressive loads in the range of axial compression ratios studied in this project have marginal effect on the shear carrying capacity of the beam-column joints. With the increase of axial compression ratio, an increased angle between the diagonal crack of the joint core concrete and the horizontal axis was observed (see Fig. 14). Moreover, it can be noted that these diagonal cracks tends to propagate into the columns. This can be attributed the increase of inclined angle of the principal stress in core concrete.

From Fig. 14, in terms of the decreasing number of cracks in the core area of the joint as well as the increased angle between the diagonal crack and the horizontal axis, it can be qualitatively concluded that under higher strain rate (e.g., 10^{-2}/s), the shear deformation in the core area of the joint consistently decreases with increasing of the axial compression ratio. Test results indicate that an increase in axial compression ratio results in an improvement of the bonding efficiency between the beam longitudinal reinforcements and core concrete of the beam-column joint, which undoubtedly restricts the cracking or damage development in the core area of the joint. Moreover, the increased axial compressive load can improve the reloading stiffness of specimen. These observations are in agreement with preliminary conclusions drawn for the quasi-static loading conditions by Fu (2002).

3.6 Strain rate level of stirrups

In order to investigate the internal stress development of the joint core area during loading, the variation of stirrup strain at same position in the core area for the strain rates of 10^{-5} and 10^{-2} are recorded and compared, as shown in Figs. 15 and 16. In these two figures, μ_Δ represents the displacement ductility factor, which can be expressed by the ratio between the applied displacement and the yielding displacement. It can be seen that in both cases, the horizontal stirrups in the core area have yielded, and the strain variation of the stirrups matches with the overall failure of the beam-column joints. Under quasi-static loading (with strain rate of 10^{-5}/s), the strain of stirrups increases with the increase of the amplitude of the cyclic displacement. After yielding of the stirrups, damage of the joint core area speeds up until the final shear failure. However, for the case of rapid loading (with strain rate of 10^{-2}/s), when the displacement ductility factor equals to 3.0, concrete in the joint core region cracks, and then the strain of stirrups grows rapidly even exceeding the yielding strain. Compared with the quasi-static loading case, the strain

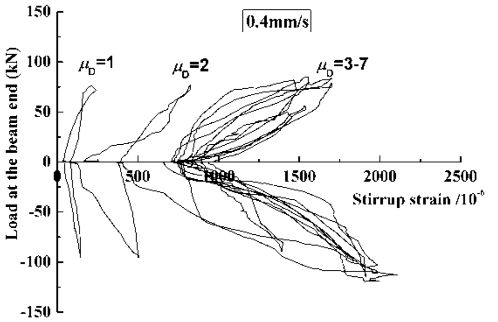

Fig. 15 Load-strain curves of the stirrup at strain rate of 10^{-5}/s

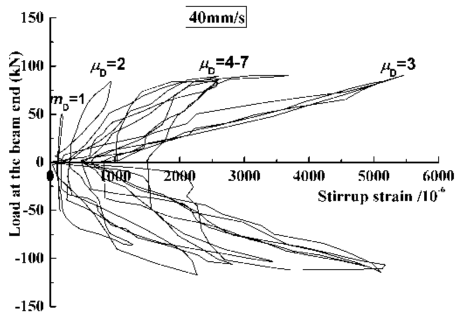

Fig. 16 Load-strain curves of the stirrup at strain rate of 10^{-2}/s

of stirrup at concrete cracking is larger. This indicates that under rapid loading, the stirrups in core area have stronger constraint on the concrete.

3.7 V_{jh}-γ relationship

The shear strain of the joint core area can be calculated through the geometric relationship of the joint deformation and the diagonal deformation measured during the test. According to the geometric relationship shown in Fig. 17, the shear angle of the joint core area can be calculated according to Eq. (4)

$$\gamma=\gamma_1+\gamma_2=\frac{\sqrt{h_j^2+b_j^2}}{h_j b_j}\frac{\delta_1+\delta_2+\delta_3+\delta_4}{2} \tag{4}$$

Based on the equilibrium of forces, the shear force of the joint core area (V_{jh}) can be predicted as

$$V_{jh}=\frac{\sum M_b}{h_{b0}-a_s'}\left(1-\frac{h_{b0}-a_s'}{H_c-h_b}\right) \tag{5}$$

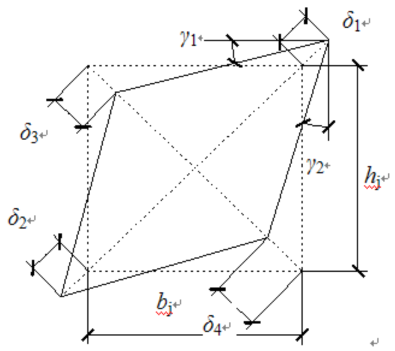

Fig. 17 Schematic diagram of the joint deformation

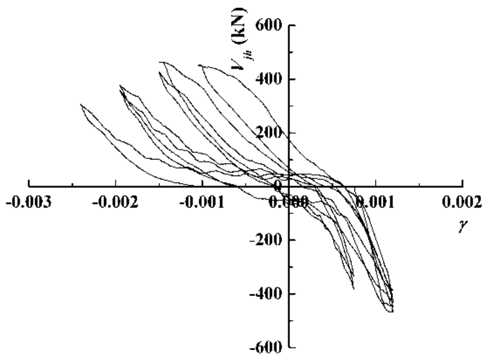

Fig. 18 V_{jh}-γ relationship of the joint at static strain rate

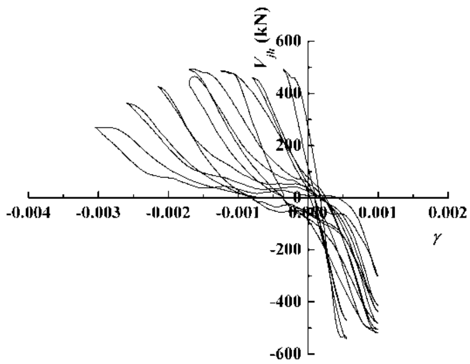

Fig. 19 V_{jh}-γ relationship of the joint at high strain rate

where H_c is the effective height of the column section; h_b is the height of the beam section; h_{b0} is the effective height of the beam section; $\sum M_b$ is a sum of the clockwise or counterclockwise bending moments around the beam section, which can be calculated by the loads acting on the beam ends; a'_s is the concrete cover of compression area. The relationships between horizontal shear carrying capacity and shear strain under quasi-static strain rate or high strain rate are shown in Figs. 18 and 19, respectively.

Under quasi-static loading, the ultimate shear strain of joint core area is 0.00225, which is smaller than that obtained under rapid loading, i.e., 0.00315 at strain rate of 10^{-2}/s. It implies that with increasing the loading rate, the shear deformation of joint core area becomes more significantly, which agrees well with observations of failure modes during testing. It can further be seen from the comparison of Figs. 18 and 19 that the ultimate horizontal shear carrying capacity under rapid loading is larger than that in the case of quasi-static loading. This can be attributed to the enhanced dynamic strength for both steel and concrete when subjected to rapid loading.

The shear carrying capacity of joint core region can be also calculated by means of the method recommended in the Chinese code for design of concrete structures (GB50011-2010) (2010)

$$V_{\mathrm{j}} = 1.1\eta_{\mathrm{j}} f_{\mathrm{t}} b_{\mathrm{j}} h_{\mathrm{j}} + 0.05\eta_{\mathrm{j}} N \frac{b_{\mathrm{j}}}{b_{\mathrm{c}}} + f_{\mathrm{yv}} A_{\mathrm{sv}} \frac{h_{\mathrm{b0}} - a'_s}{s} \tag{6}$$

in which *j* is the constraint coefficient induced by the orthogonal beams; *N* is the axial force. Other parameters can be found in Chinese code for design of concrete structures (GB50011-2010) (2010).

By applying the design parameters of the specimen into Eq. (6), the shear carrying capacity of the joint core area is calculated as 459.5 kN for the quasi-static condition. However, the measured shear carrying capacity from experiment is 448.8kN for quasi-static loading (10^{-5}/s), and 470.6 kN for rapid loading (10^{-2}/s) respectively. When the dynamic strengths of concrete and steel, which can separately be estimated by referring to CEB-FIP Model Code (1991) and Li and Li (2012), are adopted, the shear carrying capacity of the joint core area is estimated to be 533.4 kN with Eq. (6). This value is apparently higher than that obtained from test (470.6 kN). It indicates that if the dynamic strengths of concrete and steel are directly substituted into the quasi-static design model, it may overestimate the shear carrying capacity of the joint core area.

4. Conclusions

Cruciform specimens were tested to investigate the effect of loading velocity and axial compression ratio on the failure mode and carrying capacity of beam-column joints. Based on the test results presented in this paper, the following conclusions can be drawn:

• The loading velocities of 0.4 mm/s, 4 mm/s and 40 mm/s are correspondingly estimated to be 10^{-5}/s, 10^{-4}/s, and 10^{-2}/s as the strain rates on the joints. It matches well the strain orders induced by earthquake excitation.

• Test results indicate that as strain rate increases, there is no essential change in failure modes, but specimens are more inclined to brittle failure with a decrease of crack numbers. It is found that, the damage of the joint core area is serious for lower strain rate, while most damage takes place in the plastic hinge regions of the adjacent beams for higher strain rate. The slopes of post-peak branch (i.e., descending branch) of load-deflection skeleton curves increase for high loading rates.

• The axial compression ratio, ranging between 0.05 and 0.25 in this project, plays a beneficial role in the horizontal shear carrying capacity of the beam-column joints. The increased axial compression ratio can reduce the width of cracks in the joint core area, and moreover, an increased angle between the diagonal crack of the joint core concrete and the horizontal axis was observed, which is attributed the increase of inclined angle of the principal stress in core concrete.

• The shear carrying capacity of the joint core area increases as strain rate increases. The shear carrying capacity of the joint at higher loading velocity is higher than that calculated with the quasi-static method which is proposed by the design code. However, when the dynamic strengths of concrete and reinforcement, which are obtained by amplifying the static strengths with their corresponding dynamic increase factors, are directly substituted into the design model of current code, it will overestimate the shear carrying capacity of the joint core region. The dynamic increase factor of a material is treated to be dependent on the strain rate, which can be estimated with method proposed by Asprone *et al*. (2012) (see Eq. (2)).

Acknowledgements

This work was financially supported by the National Key Basic Research Program of China (973 Program) (No. 2015CB057703) and the Fundamental Reasearch Funds for the Central Universities of People’s Republic of China (No. DUT14LK23). Their support is gratefully acknowledged.

References

Asprone, D., Frascadore, R. and Ludovico, M.D. (2012), “Influence of strain rate on the seismic response of RC structures”, *Eng. Struct.*, **35**(2)**,** 29-36.
Bischoff, P.H. and Perry, S.H. (1991), “Compression behavior concrete at high strain rate”, *Mater. Struct.*, **24**(11), 425-445.
Boyce, B.L. and Dilmore, M.F. (2009), “The dynamic tensile behavior of tough, ultrahigh-strength steels at strain-rates from $0.0002s^{-1}$ to $200s^{-1}$”, *Int. J. Impact Eng.*, **36**(2), 263-271.
CEB-FIP Model Code (1990, 1991), Comité Euro-International du Béton.
Cusatis, G. (2011), “Strain-rate effects on concrete behavior”, *Int. J. Impact Eng.*, **38**(4), 162-170.
Fu, J.P. (2002), “Seismic behavior and design of joints in a reinforced concrete frame”, Ph.D. Dissertation,

Chongqing University.
GB50010 (2010), *Code for design of concrete structures*, Construction Ministry of China.
Ghobarah, A. and Biddah, A., (1999), "Dynamic analysis of reinforced concrete frames including joint shear deformation", *Eng. Struct.*, **21**(11), 971-987.
Hakuto, S., Park, R. and Tanaka, H. (2000), "Seismic load test on interior and exterior beam-column joints with substandard reinforcing details", *ACI Struct. J.*, **97**(1), 11-24.
Hasan, A.S.M.Z., Hamid, R. and Ariffin, A.K. (2010), "Stress-strain behavior of normal strength concrete subjected to high strain rate", *Asian J. Appl. Sci.*, **3**(2), 145-152.
Isaac, P., Darby, A., Ibell, T. and Evernden, M. (2013), "Influence of loading rate on failure mode of reinforced concrete members", *Proc. ICE-Eng. Comput. Mech.*, **166**(4), 194-203.
Lee, W.S. and Lin, C.F. (1998), "Plastic deformation and fracture behaviour of Ti-6Al-4V alloy loaded with high strain rate under various temperatures", *Mater. Sci. Eng.*, ASCE, **241**(1-2), 48-59.
Lee, W.S., Shyu, J.C. and Chiou, S.T. (2000), "Effect of strain rate on the impact response and dislocation substructure of 6061-T6 aluminum alloy", *Scripta Materialia*, **42**, 51-56.
Li, M. and Li, H.N. (2012), "Effects of strain rate on reinforced concrete structure under seismic loading", *Adv. Struct. Eng.*, **15**(3), 461-475.
Li, B. and Tran, C.T.N. (2009), "Seismic behaviour of reinforced concrete beam-column joints with vertical distributed reinforcement", *ACI Struct. J.*, **106**(6), 790-799.
Li, B., Tran, C.T.N. and Pan, T.C. (2009), "Experimental and numerical investigations on the seismic performance of lightly reinforced concrete joints", *J. Struct. Eng.*, ASCE, **135**(9), 1007-1018.
Lu, X., Urukap, T.H., Li, S. and Lin, F. (2012), "Seismic behavior of interior RC beam-column joints with additional bars under cyclic loading", *Earthq. Struct.*, **3**(1), 37-57.
Malvar, L.J. and Ross, C.A. (1998), "Review of strain rate effects of concrete in tension", *ACI Mater. J.*, **95**(6), 735-739.
Manjoine, M.J. (1944), "Influence of rate of strain and temperature on yield stress of mild steel", *J. Appl. Mech.*, **11**, 211-218.
Martínez, J.A.R., Rusinek, A. and Klepaczko, J.R. (2009), "Constitutive relation for steels approximating quasi-static and intermediate strain rates at large deformations", *Mech. Res. Comun.*, **36**(4), 419-427.
Meas, K., Li, B. and Pham, T.P. (2014), "Experimental and Numerical Studies on the Seismic Performance of RC Interior Beam-Column Joints", *Adv. Struct. Eng.*, **17**(2), 233-247.
Mukai, T., Ishikawa, K. and Higashi, K. (1995), "Influence of strain rate on the mechanical properties in fine-grained aluminum alloy", *Mater. Sci. Eng.*, ASCE, **204**(1-2), 12-18.
Shah, S.P., Wang, M.L. and Chung, L. (1987), "Model concrete beam-column joints subjected to cyclic loading at two rates", *Mater. Struct.*, **20**(2), 85-95.
Sharma, A., Eligehausen, R. and Reddy, G. (2011), "A new model to simulate joint shear behavior of poorly detailed beam-column connections in RC structures under seismic loads, Part I: exterior joints", *Eng. Struct.*, **33**(3), 1034-1051.
Sun, H.B., Yoshida, F. and Ohmori, M. (2003), "Effect of strain rate on Lüders band propagating velocity and Lüders strain for annealed mild steel under uniaxial tension", *Mater. Lett.*, **57**(29), 4535-4539.
Takeda, J.I. (1984), "Dynamic fracture of concrete structures due to severe earthquakes and some consideration on countermeasures", *Proceedings of the 8th World Conference on Earthquake Engineering*, San Francisco, California, USA.
Yadar, S. and Ramesh, K.T. (1995), "The mechanical properties of tungsten-based composites at very high strain rates", *Mater. Sci. Eng.*, ASCE, **203**(1-2), 140-153.

CC